International Journal of Pharmaceutics 692 (2026) 126629

Contents lists available at ScienceDirect

International Journal of Pharmaceutics

journal homepage: www.elsevier.com/locate/ijpharm

Engineering lipid-coated silica nanoparticles as versatile adjuvant delivery platform for the TLR4 agonist MPLA

Andreas G. Schreiber [a], Johannes Konrad [a], Renate Liebl [a], Bastian Beitzinger [b], Jan Krutina [c], Gregor Madej [c], Mika Lindén [b], Christine Ziegler [c], Miriam Breunig [a,*]

[a] Department of Pharmaceutical Technology, University of Regensburg, Universitaetsstrasse 31, 93053 Regensburg, Germany
[b] Institute of Inorganic Chemistry II, University of Ulm, Albert-Einstein-Allee 11, 89081 Ulm, Germany
[c] Department of Structural Biology/ Biophysics II, University of Regensburg, Universitaetsstrasse 31, 93053 Regensburg, Germany

ARTICLE INFO

Keywords:
MPLA
Silica nanoparticles
Mesoporous silica nanoparticles
Lipid coating
Bayesian optimization
TLR4 activation

ABSTRACT

Lipid-coated solid and mesoporous silica nanoparticles (LC-SiNPs and LC-MSNs) were developed as modular platform for the delivery of Toll-like receptor (TLR) agonists. In this study, the incorporation of the amphiphilic TLR4 agonist monophosphoryl lipid A (MPLA) into lipid bilayers of the newly developed platform was systematically optimized. Both core particle types -solid and mesoporous- provided a stable surface structure to enhance membrane stability. By varying cholesterol (15–45%) and anionic lipid (DPPG) (10–30%) content, we identified key composition parameters that influence TLR4 activation, membrane fluidity and particle-cell interactions. Solid-core MPLA-SiNPs showed enhanced immunostimulatory activity compared to unformulated MPLA when formulated with cholesterol levels increased to 45% and moderate DPPG fractions of 20%, while mesoporous MPLA-MSNs required higher DPPG content of 30% for comparable activation. To further refine performance, Bayesian optimization (BO) was applied, leading to a significant improvement in MPLA-SiNPs. The BO-optimized MPLA-SiNPs achieved an EC_{50} value of 87 ng/mL, outperforming classical formulation strategies. This optimized EC_{50} was 60 ng/mL lower than for the particles optimized using the classical One-Factor-At-a-Time approach and 280 ng/mL lower compared to unformulated MPLA. Macrophages as antigen-presenting cells carrying TLR4 receptors efficiently internalized and processed the particles. These findings underscore the importance of rational formulation design and demonstrate the potential of lipid-coated silica nanoparticles as modular vaccine carriers. This versatile and modular platform can in future be exploited for delivery of other TLR agonists and additionally be equipped with antigens.

1. Introduction

Adjuvants such as Toll-like receptor (TLR) agonists stimulate the innate immune system and have an additional leverage effect for poor immunogens in the process of adaptive immune response (Kaur et al., 2022; Pulendran et al., 2021). To achieve relevant concentrations in draining lymph nodes to activate immune cells in the context of adaptive immune cells, nano-sized carriers with a size preferably below 200 nm are applied for TLR agonist delivery (Oussoren et al., 1997; Swartz et al., 2008; Reddy et al., 2007; Manolova et al., 2008). Although numerous TLR agonist formulations on the nano-scale exist (Gu et al., 2024; Hamid et al., 2025; Naz et al., 2025; LaBauve et al., 2018), they are typically tailored to a single specific TLR agonist. However, selecting a different TLR agonist requires developing a new formulation. Our goal was to advance the field by creating a delivery platform that allows for easy exchange of TLR agonists and, in future, additional incorporation of antigens.

As a proof-of-concept we decided to develop a formulation for the TLR4 agonist monophosphoryl lipid A (MPLA). MPLA finds application in several licensed prophylactic vaccines like Fendrix® (hepatitis B virus) (Hernán-García et al., 2025), Cervarix® (human papillomavirus −16 and −18) (D'Onofrio et al., 2025), RTS,S® (Malaria) (Friedman-Klabanoff et al., 2025), and Pollinex® Quattro (grass pollen allergy) (Zimmermann et al., 2022). In approved vaccines, MPLA is incorporated into adjuvant systems (AS), such as liposome-based AS01, oil-in-water emulsion AS03, or alum-adsorbed AS04 (Laupèze et al., 2019). The development of a MPLA formulation is challenging because on the one hand parameters like a high loading and sufficient stability during

* Corresponding author.
E-mail address: miriam.breunig@ur.de (M. Breunig).

https://doi.org/10.1016/j.ijpharm.2026.126629
Received 5 November 2025; Received in revised form 9 January 2026; Accepted 26 January 2026
Available online 5 February 2026

transport are required (Peletta et al., 2023), but on the other hand a monomeric availability of MPLA is necessary for receptor activation (Du et al., 2024). Therefore, once arrived at its target cells, MPLA has to be "extracted" from the formulation and be presented in its monomeric form with the help of adaptor protein MD-2 to its extracellular TLR4 receptor (Du et al., 2024; Botos et al., 2011; Ignacio et al., 2018). This is challenging because MPLA is an amphiphilic molecule with a very low critical micellar concentration (10^{-9} mol/L) (Liu et al., 2017), and therefore, exists rather as aggregated structures in physiological environment (Du et al., 2024).

For our delivery platform, we have decided to rely on silica nanoparticles as they fulfill the upper size limit for lymph node transport of about 200 nm, are biocompatible and biodegradable, and can be easily modified on their surface (Navarro-Tovar et al., 2016). We have already exploited solid silica nanoparticles (SiNPs) for the immobilization of the envelope antigen of HIV-1 and receptor binding domain (RBD) of SARS-CoV-2, respectively, in a well-defined and orientated manner (Barbey et al., 2023; Thalhauser et al., 2020). In addition to solid SiNPs, we have selected mesoporous silica nanoparticles (MSNs) that have a well-defined inner pore structure with tunable pore sizes ranging from 2 to 50 nm depending on the synthesis strategy (Navarro-Tovar et al., 2016; Li et al., 2018). The pores allow for control over degradation time (Croissant et al., 2017), and may for example be tailored to host an additional active molecule. We hypothesize that coating silica-based nanoparticles with a liposomal membrane will create a modular delivery platform that combines the structural stability and size control of silica nanoparticles with the compositional versatility of liposomes (Navarro-Tovar et al., 2016; B. Vörös-Horváth, A. Salem, B. Kovács, A. Széchenyi, S. Pál, Systematic Study of Reaction Conditions for Size-Controlled Synthesis of Silica Nanoparticles, Nanomaterials (Basel, Switzerland) 14, 2024; Nsairat et al., 2022). The rigid structure of silica cores ensures size uniformity and prevents coalescence, which is a common drawback of liposomes during storage and transport (Mizuta et al., 2023; Patel et al., 2020). Depending on whether we used solid SiNPs or mesoporous MSNs, we denote our lipid-coated particles as either LC-SiNPs or LC-MSNs, respectively.

The lipid membrane on LC-SiNPs and LC-MSNs was exploited for incorporation of amphiphilic MPLA. To modulate on the one hand a sufficiently stable emplacement of MPLA in the lipid bilayer, and on the other hand its release for eliciting an effect at TLR4, our goal was to identify optimal liposomal membrane formulations using zwitterionic dipalmitoylphosphatidylcholine (DPPC, a lecithin), anionic dipalmitoylphosphatidylglycerol (DPPG), and cholesterol at various ratios. For some formulations, also PEGylated distearoylphophatidylethanolamine (DSPE-PEG) was employed to enhance colloidal stability (LaBauve et al., 2018). In a first step, the cholesterol content of the liposomal membrane was varied due to its influence on membrane fluidity (Subczynski et al., 2017; Kaddah et al., 2018). In a second step, the charge density of the nanoparticles was varied by changing the number of anionic compounds DPPG and MPLA. The electrostatic repulsion affects not only the colloidal stability by hindering approach between particles but also has influence on the interaction with cells (Sanità et al., 2020). With such a classical One-Factor-At-a-Time optimization the effect of only one variable is observed, and the impact of how factors mutually influence each other remains unidentified (Gisperg et al., 2025). Consequently, only a local optimum may be identified instead of a global one. This obstacle can be avoided by Bayesian optimization (BO) (Gisperg et al., 2025). BO can deal with stochastic noise and integrates Machine Learning with adaptive sampling into a global optimization algorithm. Therefore, we exploited BO for final optimization of our formulations, and tested their biological effect compared to unformulated MPLA on TLR4-expressing reporter cells in vitro as measure of available amount of the adjuvant. In this context, availability means not only the concentration of MPLA, but also the feasibility to be extracted from lipid membranes for TLR4 activation, and thus the existence in its monomeric form.

2. Materials and methods

2.1. Materials

All chemicals were obtained from Sigma-Aldrich (Taufkirchen, Germany), unless stated otherwise. Solid 100 nm SiNPs (sicastar® white and sicastar® greenF suspensions) were purchased from micromod Partikeltechnologie GmbH (Rostock, Germany). Sodium chloride (p.a.) and cholesterol (≥95%) were sourced from Carl Roth (Karlsruhe, Germany). Synthetic MPLA was acquired from InvivoGen (Toulouse, France). RPMI 1640 medium, L-glutamine and penicillin-steptomcyin were obtained from Thermo Fisher Scientific (Darmstadt, Germany). Crylon® extruded poly(methyl methacrylate) wafers, 2 mm thick, were provided by KMH Kunststoff Metallhandel GmbH & Co. KG (Regensburg, Germany). Resatorvid was received as a complimentary sample from MedChem Express (Monmouth, USA). 1,2-Dipalmitoyl-*sn*-glycero-3-phosphocholine (DPPC) and 1,2-dipalmitoyl-*sn*-glycero-3-phospho-*rac*-glycerol sodium salt (DPPG) were kindly provided by Lipoid (Ludwigshafen, Germany). Ultrapure water was produced using a Milli-Q water purification system (Merck Millipore, Germany).

2.2. Synthesis of MSNs

In a 500 mL round-bottomed flask equipped with magnetic stirring, 1.294 g cetyltrimethylammonium bromide was dissolved in a mixture of 320 g demineralized water and 80 g ethanol. The mixture was homogenized at 50°C under stirring (500 rpm) for 30 min. 2.0 mL tetraethyl orthosilicate was then added, and after 5 min of continued stirring, sodium hydroxide solution (1 M, 1.1 mL) was introduced. The reaction was maintained at 50°C for 1 h, after which heating was discontinued and the mixture was stirred at room temperature for 18 h. MSNs were precipitated by adding ammonium nitrate to the reaction mixture, collected by centrifugation (7,500 rcf, 15 min), and washed by redispersing the pellet in ethanol via bath sonication for 30 min. The solids were re-collected by centrifugation (7,500 rcf, 15 min), dried, gently ground to a fine powder, and calcined at 550°C for 5.5 h with a 5 h heating ramp.

2.3. Fabrication of microfluidic systems

The design for microfluidic production of liposomes by flow focusing with high aspect ratios was adapted from Hood and DeVoe (2015). Briefly, the microfluidic system consisted of three sample ports (Fig. S1). The middle stream of lipids dissolved in ethanol was focused by the two aqueous buffer channels. As the ethanol rapidly mixed with the buffer, the lipids could no longer be dissolved and uniform liposomes formed (Hood and DeVoe, 2015; Akar et al., 2024).

Microfluidic chips were fabricated with a laser-engraving device VLS 2.30 equipped with a 30 W CO_2 laser ($\lambda = 10.6$ μm) from Universal Laser Systems (Universal Laser Systems Inc., Scottsdale, Arizona, USA). The chip design (shown in Fig. S1) was drawn in original size with vector graphic software CorelDRAW 24 (Corel Corporation, Ottawa, Ontario, Canada). The Corel Draw data are compatible without any conversion with the laser engraving device. The channels (≈150 μm wide) were cut into 3 x 6 cm PMMA slabs by engraving twice at 90% laser power and 16% scribing speed (maximum speed is 0.127 m/s). For the sample inlets as well as the product outlet, the speed was set to 90% and the laser power set to 42%. The image density parameter was adjusted to level 7 which equals 1000 pulses per inch (PPI) in x-direction and 2000 PPI in y-direction, respectively. The PMMA wafers were cleaned with isopropyl alcohol and compressed air to remove dust traces within the channels. The chips were closed with sterile SealPlate® microplate sealing film. In the sample and exit ports, PTFE tubes with 0.6 mm inner and 1.3 mm outer diameter were fixed with hot glue melt. The entire chip was glued onto another PMMA slab for mechanical support. Prior to use, the microfluidic devices were flushed for at least 15 min with ethanol p.a. at

a low flow rate for final cleaning.

2.4. Preparation of liposomes

Stock lipids were prepared in ethanol p.a. at concentrations of 10 mg/mL and mixed according to the desired composition. The microfluidic system was operated at a total flow rate of 12 mL/min and an isotonic NaCl:ethanol flow rate ratio of 8:1. The final liposome suspension was collected and used without any further purification.

2.5. Fabrication of LC-SiNPs & LC-MSNs and adjuvantation with MPLA

Coating of SiNPs and MSN was performed in isotonic NaCl solution adapted from established protocols (LaBauve et al., 2018; Moura and Carmona-Ribeiro, 2005; Durfee et al., 2016). Liposomes were combined with the core particles in a 1.4-fold excess to the core particles with regard to their surface area determined by NTA. The particle suspension was diluted with isotonic NaCl to a silica concentration of 1 mg/mL and sonicated for 30 min with an Emmi 85HC ultrasonic cleaner (Mörfelden-Waldorf, Germany). The coated particles were separated from "empty" liposomes by centrifugation at 9,000 rcf for 9 min at 20°C. The particle pellet was redispersed in the desired volume with isotonic NaCl. For cell uptake experiments, green fluorescent SiNPs were employed, and the adsorbed liposomal membranes were stained with DiD in an approximately 1:500 dye:lipid ratio. For the incorporation with the adjuvant, MPLA dissolved in 1:1 DMSO:H_2O was pre-diluted with NaCl solution, and the coated particles were added. After 30 min incubation to let MPLA penetrate the membrane, the particles were again centrifuged (9,000 rcf, 9 min, 20°C) and separated from the supernatant.

2.6. Characterization of nanoparticles

Zeta potentials and hydrodynamic diameters as well as polydispersity indices (PDI) were determined with a Zetasizer Nano ZS (Malvern Instruments, Kassel, Germany). While size measurements could be performed in isotonic NaCl solution, for zeta potential analysis, a lower ionic strength was necessary. Hence, the measurement was performed with the diffusion barrier method. The cuvettes were prefilled with 1/20 diluted NaCl solution and the sample was diluted 1/4 with water. 100 µL of the diluted sample was then injected to the bottom of the cuvette as a plug. Nanoparticle concentration analysis and measurement of the particle surface was conducted by nanoparticle tracking analysis (NTA) on a NanoSight NS300 (Malvern Panalytical, Kassel, Germany).

Nitrogen sorption experiments were performed at −196°C using a Quadrasorb-1 (Quantachrome Instruments, Germany) after drying the samples under vacuo at 100°C for 22 h. Pore size distributions were derived with the equilibrium NLDFT kernel (silica, cylindrical pores) over a relative pressure range of 0–0.9, and pore volumes were taken at a relative pressure of 0.9. Specific surface areas were estimated by the t-plot approach within the relative pressure interval of 0.75–0.95.

For the adsorption isotherm, LC-SiNPs were prepared as described above with varied amounts of liposomes added. The supernatants after centrifugation were collected, diluted with 0.5 M nitric acid, and subjected to phosphorus inductively coupled plasma atomic emission spectroscopy (ICP-OES) on a SPECTROBLUE FMX36 (SPECTRO Analytical Instruments GmbH, Kleve, Germany).

Membrane fluidity of LC-SiNPs and LC-MSN was determined by anisotropy of the fluorescent probe 1,6-diphenyl-1,3,5-hexatrien in a ratio of 1:500 DPH:lipid ratio according to (He, 2023) on a temperable Jasco FP-6300 (Jasco, Pfungstadt, Germany) spectrofluorometer equipped with a polarizer and an analyzer. The G-factor (ratio of the sensitivities of the detector for vertically and horizontally polarized light) was determined for each sample.

Cryo-TEM imaging was performed on an in-house JEOL CRYO ARM™ 200 (JEOL Inc. Tokyo, Japan). Aliquots of sample (4 mg/mL) were prepared for cryo-electron microscopy (cryo-EM) imaging. Three microliters of the sample solution were applied to glow-discharged Quantifoil R 1.2/1.3 holey-carbon grids (300 mesh). The grids were blotted using a Laika GP2 grid-plunger under controlled conditions of 4°C and 85% relative humidity. The grids were then immediately plunge-frozen into liquid ethane to achieve vitrification.

Cryo-EM data collection was performed using a transmission electron microscope (JEOL cryoARM-200) operated at 200 kV and a K2 Summit direct electron detector (Gatan). A GIF energy filter, operating with a 20 eV slit width, was utilized to enhance image contrast by removing inelastically scattered electrons. Data acquisition followed a standard protocol, which included automated low-magnification grid mapping and subsequent high-magnification image collection. For overview imaging, data was acquired at a nominal magnification of 8,000x. Images were collected with an exposure time of 0.8 s (1 frame), resulting in a pixel spacing of 5.828 Å. The dose rate was 2.5 e^-/pixel/s, and images were collected at a nominal defocus of 0 µm (eucentric height). Overview images were acquired as a composited 4x4 image shift montage. High-resolution micrographs were collected at a nominal magnification of 60,000x. The images were recorded over an exposure time of 3.0 s, comprising 38 total frames, with a pixel spacing of 0.7891 Å. The dose rate was set to 6.2 e^-/pixel/s. The target defocus was set to −1.8 µm.

2.7. Cell culture and cell lines

HEK-Blue™ hTLR4 reporter cells were purchased from InvivoGen (Toulouse, France). Briefly describing the cell line, human embryonic kidney 293 (HEK293) cells were co-transfected with the human TLR4, MD-2 and CD14 genes and an NF-κB-inducible secreted embryonic alkaline phosphatase (SEAP) reporter gene. Activation of the TLR4 resulted in the expression and secretion of the enzyme which caused a color change from regular red media color into purple/blue in HEK-Blue™ detection media. The cells were cultured in high-glucose Dulbecco's modified Eagle's medium supplemented with 4 mM L-glutamine, 10% low endotoxin, heat-inactivated fetal calf serum, and 1x HEK-Blue™ selection (InvivoGen) according to the supplier's instructions. When the cells reached confluency of approximately 80%, they were subcultured. Maintenance was taken at 37°C in a humidified atmosphere with 5% CO_2. The reporter assay was performed at a cell density of 55×10^3 cells/ well and elsewise according to the manufacturer's instructions. Photometric read out at 620 nm took place after 23–24 h incubation with a Fluostar Omega plate reader (BMG Labtech, Ortenberg, Germany).

THP-1 cells (55×10^3 cells/well) were seeded into an 8-well slide (ibidi, Planegg, Germany) and differentiated into macrophages by treatment with 0.1 µM phorbol-12-myristate-13-acetate (PMA). Cells were cultured for 48 h at 37°C in a humidified atmosphere containing 5% CO_2 using RPMI 1640 medium supplemented with 10% low-endotoxin heat-inactivated fetal bovine serum, 2 mM L-glutamine, 1× non-essential amino acids, 1 mM sodium pyruvate, 1× vitamins and 1000 U/mL penicillin–streptomycin. Prior to the experiment, differentiated macrophages were washed with 1× PBS and resuspended in fresh culture medium containing double-stained LC-SiNPs at a final concentration of 360×10^3 particles per cell. After incubation periods ranging from 3 to 48 h, the supernatant containing uninternalized particles was removed, and cells were washed twice with PBS.

Macrophages were then fixed with 4% paraformaldehyde for 15 min, followed by three PBS washes. Nuclei were stained with 200 µL of DAPI (10 µg/mL) for 25 min, and excess stain was removed by two additional PBS washes.

Prepared samples were mounted with glycergel mounting medium and imaged using a LSM 710 confocal microscope (Zeiss, Oberkochen, Germany). Image analysis was performed using Zeiss Zen Lite software (Zeiss, Oberkochen, Germany).

2.8. Bayesian optimization

Bayesian optimization was conducted using the BOXVIA software (Ishii et al., 2022). In brief, EC_{50} values from previously tested formulations were input into the program. The batch size (the number of formulations to be suggested per iteration) was set to four, and the acquisition function was configured to "enhanced improvement." The Matern 5/2 kernel was selected for modeling. Formulation constraints were defined as follows: cholesterol content between 15 and 45% and DPPG between 10 and 30%, both in 5% increments; MPLA was allowed within a range of 1.5–10%, in 0.5% increments. The optimization algorithm was executed twice for each particle type: the first run employed a jitter value of 10, and the second run used a jitter of 1. Results from the initial run were fed back into the program to inform the second iteration.

2.9. Statistical analysis

All data are presented as mean ± standard deviation of triplicate measurements, or mean ± propagated error if Gaussian error

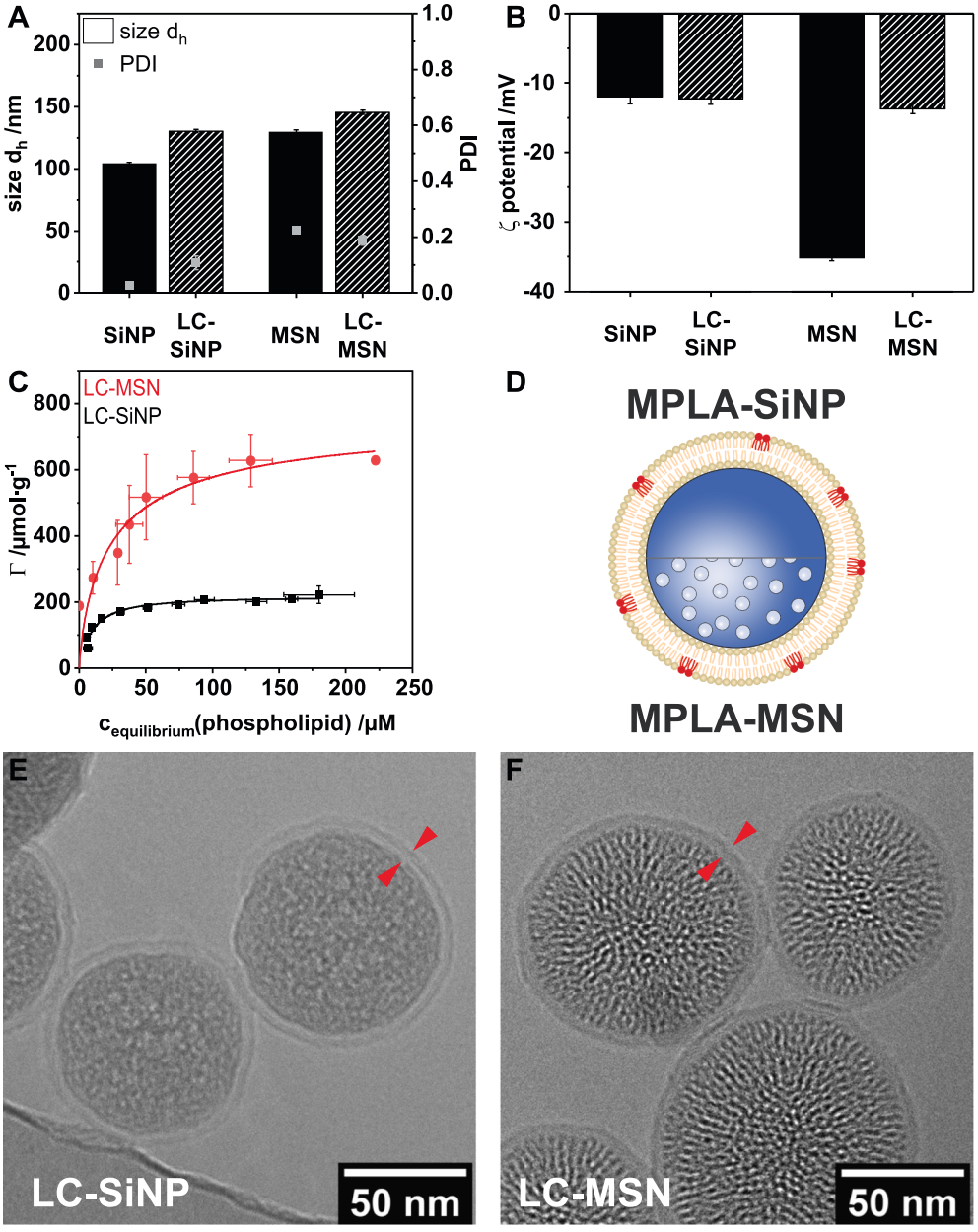

Fig. 1. Characterization of silica nanoparticles before (SiNPs and MSNs) and after (LC-SiNPs and LC-MSNs) coating with liposomal membranes. The lipid composition was 45% zwitterionic DPPC, 20% anionic DPPG and 35% cholesterol for LC-SiNPs, and 52.5:30:15:2.5 DPPC:DPPG:chol:DSPE-PEG for LC-MSNs. A) After the coating process, the hydrodynamic diameter increased by about 26 nm (LC-SiNPs) and 35 nm (LC-MSNs). The PDI of LC-SiNPs did not exceed 0.1, while it was even reduced for LC-MSNs to 0.19 from initially > 0.2 as determined by DLS. B) The zeta potential was about −12 to −14 mV for LC-SiNPs, and was thus similar to uncoated SiNPs. LC-MSNs showed a zeta potential of about −15 mV. C) The adsorption isotherm was determined by phosphorus ICP-OES. The fit according to Langmuir theory revealed a complete surface coverage with 211 µmol/g (only phospholipids determined), which transfers to 325 µmol/g total lipid including cholesterol for LC-SiNPs, and 633 µmol/g (only phospholipids) or 744 µmol/g including cholesterol for LC-MSNs. D) Scheme of a MPLA-SiNP (top half) and MPLA-MSN (bottom half). The core particles (blue) are coated with a liposomal membrane (yellowish) in which MPLA (red) is incorporated. E,F) Cryo-TEM imaging further proved adsorption of a single bilayer membrane on the core particles. Red arrows point out examples of the membrane with an apparent thickness of 5.6 (± 0.8) nm (LC-SiNPs) and 5.7 (± 0.8) nm (LC-MSNs). Data are expressed as mean ± uncertainty.

propagation was applicable. Statistical analyses and curve fittings were performed with Origin 2023b software (OriginLab Corporation, Northampton, Massachusetts, USA).

3. Results

3.1. Fabrication and characterization of LC-SiNPs and LC-MSNs and insertion of MPLA

Solid SiNPs and mesoporous MSNs were each coated with a liposomal membrane to generate LC-SiNPs and LC-MSNs. For the fabrication of liposomes, a lipid mixture composed of neutral DPPC, cholesterol, and negatively charged DPPG at a molar ratio of 45:35:20 was applied. The hydrodynamic diameter of uncoated SiNPs and MSNs was 104 (± 1) nm and 130 (± 2) nm, respectively (Fig. 1a). MSNs had center-radially aligned pores with a narrow size distribution of around 3.7 nm in diameter with a pore volume 0.5 cm^3/g (determined at $p/p_0 = 0.8$) (data not shown). Porosity of the MSNs was evaluated by nitrogen adsorption. The specific surface area was 862 m^2/g, while the external area was 123 m^2/g (data not shown). After adsorption of the lipid bilayer, the diameter increased to about 130 nm (LC-SiNPs) and to about 145 nm (LC-MSNs), respectively. The resulting particles demonstrated excellent homogeneity, with polydispersity indices (PDIs) of 0.11 ± 0.02 (LC-SiNPs) and 0.19 ± 0.02 (LC-MSNs). Both coated particle species showed negative zeta potentials of about −12 to −14 mV (Fig. 1b). Langmuir adsorption isotherms were used to calculate the maximum amount of phospholipids possibly adsorbed on the particle surface, resulting in 211 (± 3) μmol/g (SiNPs) and 633 (± 55) μmol/g (MSNs) (Fig. 1c). The total adsorbed lipid amount including cholesterol was thus 325 (± 5) μmol/g for SiNPs and 744 (± 65) μmol/g for MSNs. The colloidal stability and zeta potential of LC-SiNPs and LC-MSNs showed only minimal changes in the pH range of 5 to 8 (Fig. S2a,b). Furthermore, the colloidal stability of LC-SiNPs was maintained in various buffers at 4°C for at least one month, and in buffers as well as in serum supplemented cell culture medium for a minimum of one week at 37°C (Fig. S2c,d). Cryo-TEM microscopy confirmed the adsorption of a single lipid bilayer on the surface of SiNPs and MSNs (Fig. 1e,f), with membrane diameters of approximately 6 nm independent on the supporting nanoparticle (micrographs of uncoated SiNPs and MSNs next to LC-SiNPs and LC-MSNs are shown in Fig. S3a,b). The depiction of a liposome in Fig. S3b further confirms that the structures observed on the silica surfaces correspond to adsorbed lipid bilayers rather than an optical artefact. Size distributions (Fig. S3c,d) of particles in cryo-EM micrographs were 86 (± 11) nm (LC-SiNPs) and 105 (± 16) nm (LC-MSNs), which were as expected smaller than the hydrodynamic diameters.

The LC-SiNPs and LC-MSNs prototype formulations were selected for insertion of the amphiphilic MPLA into the lipid bilayer at a ratio of 1.5% (Fig. 1d). MPLA remained stably incorporated into the lipid membrane of SiNPs for at least one week (Fig. S4). Adjuvanted particles were comparable in size and PDI in various buffers as well as in serum supplemented cell culture medium to their parent particles.

3.2. Effect of the membrane fluidity on the biological effect of MPLA-SiNPs and MPLA-MSNs

In a first step, the cholesterol content of MPLA-SiNPs and MPLA-MSNs was varied from 15% to 45%, while the fraction of the anionic lipid DPPG was maintained at 10%. The particles were adjuvanted with 1.5% MPLA relative to the total lipid content. Physicochemical characterization of all particles is shown in Fig. S5a–f. Formulations that exceeded 200 nm in diameter and are thus not applicable for lymph node transport during vaccination are marked with an asterisk in Fig. 2a-c.

The ability of MPLA that was formulated in particles or applied in free/unformulated form to stimulate TLR4 was evaluated by using HEK-TLR4 positive reporter cells. The subsequent NFκB-activation was determined by an enzymatically induced color change in the supernatant. In the series of solid MPLA-SiNPs, stimulation of TLR4 increased with increasing cholesterol content of the lipid membrane (Fig. 2a). At the same time EC_{50} values decreased by 130 ng/mL. MPLA-SiNPs formulated with 35% and 45% cholesterol showed a similar half-maximal activation comparable to unformulated MPLA, though they reached a lower plateau of the maximal cell response. However, none of these MPLA-SiNPs formulations had a lower EC_{50} value compared to unformulated MPLA, and thus at least the same or even a higher concentration of adjuvant had to be employed to elicit the same TLR4 activation.

Because mesoporous MPLA-MSNs tended towards aggregation, they were stabilized either electrostatically with 2 mM $MgCl_2$ added to the buffer (MPLA-MSN_{MgCl2}, Fig. 2b), or sterically by the addition of 2.5% PEGylated lipids to the membrane (MPLA-MSN_{PEG}, Fig. 2c). In contrast to MPLA-SiNPs with a solid core, the trend of receptor activation of MPLA-MSN_{MgCl2} was vice versa, it increased with decreasing cholesterol content. MPLA–MSN_{MgCl2} with a low cholesterol content of 15% elicited the lowest EC50 that was comparable to free MPLA. But again, none of the MPLA-MSN_{MgCl2} formulations surpassed unformulated MPLA in TLR4 activation. The variation of cholesterol content revealed no trend for MPLA–MSN_{PEG}. All EC50 values, including the one obtained from unformulated MPLA, were in the range of 370 to 440 ng/mL, and thus no MPLA-MSN_{PEG} formulation outperformed free MPLA.

The membrane fluidity depending on the cholesterol content of the lipid membrane was monitored by anisotropy of the fluorescent probe DPH. Up to physiological temperature of 37°C at which the reporter assay was performed, membrane fluidities were comparable for all formulations (marked by a vertical dotted line in Fig. 2d-f). Thus, the effect of cholesterol content of MPLA-SiNPs and MPLA-MSNs on TLR4 activation was not driven by membrane fluidity. At higher temperatures however, differences between the formulations became visible and, thus the main phase transition temperature (T_m) was determined by the inflection point of a Boltzmann fit of the anisotropy data. For MPLA-SiNPs, T_m increased from 49.0°C to 63.3°C with increasing cholesterol fraction up to 35% at which it plateaued (Fig. 2d, Table S1). Though MPLA-MSN_{MgCl2} containing low cholesterol (15%) had similar T_m compared to corresponding MPLA-SiNPs, the increase of T_m was more pronounced as it reached > 70°C at 45% cholesterol content. In contrast, MPLA-MSN_{PEG} experienced only an increase up to 61.8°C in T_m for the highest cholesterol content. However, as T_m were above 37°C, they did not directly influence the results.

For further optimization, solid MPLA-SiNPs with 45% cholesterol and mesoporous MPLA-MSNs with 15% cholesterol were selected as those formulations achieved the best TLR4 activation and fulfilled the size criterion as well.

3.3. Effect of the surface charge on the biological effect of MPLA-SiNPs and MPLA-MSNs

In a next step, optimal cholesterol contents were fixed as evaluated for each particle species (MPLA-SiNPs: cholesterol 45%, MPLA-MSNs: 15%), and the influence of the anionic components DPPG and MPLA was investigated. The lipid DPPG was varied from 10% to 30%, and MPLA was applied in quantities ranging from 1.5% to 10%.

Overall, variation of the MPLA loading had only a minor or no effect on the receptor activation for all formulations, independent of the particle core or the DPPG content (light to dark blue curves in Fig. 3).

In the series of MPLA-SiNPs, all formulations with 10% DPPG and 20% DPPG shifted to the left compared to free MPLA indicating an overall improved TLR4 receptor response and a lower amount of MPLA necessary to elicit the same response (Fig. 3a,b). This effect was even more pronounced for particles containing 20% DPPG. In contrast, a further increase of the anionic lipid fraction to 30% led to no enhanced receptor activation compared to unformulated MPLA (Fig. 3c). Among the MPLA-SiNPs, the formulation with 35:45:20 DPPC:Chol:DPPG plus

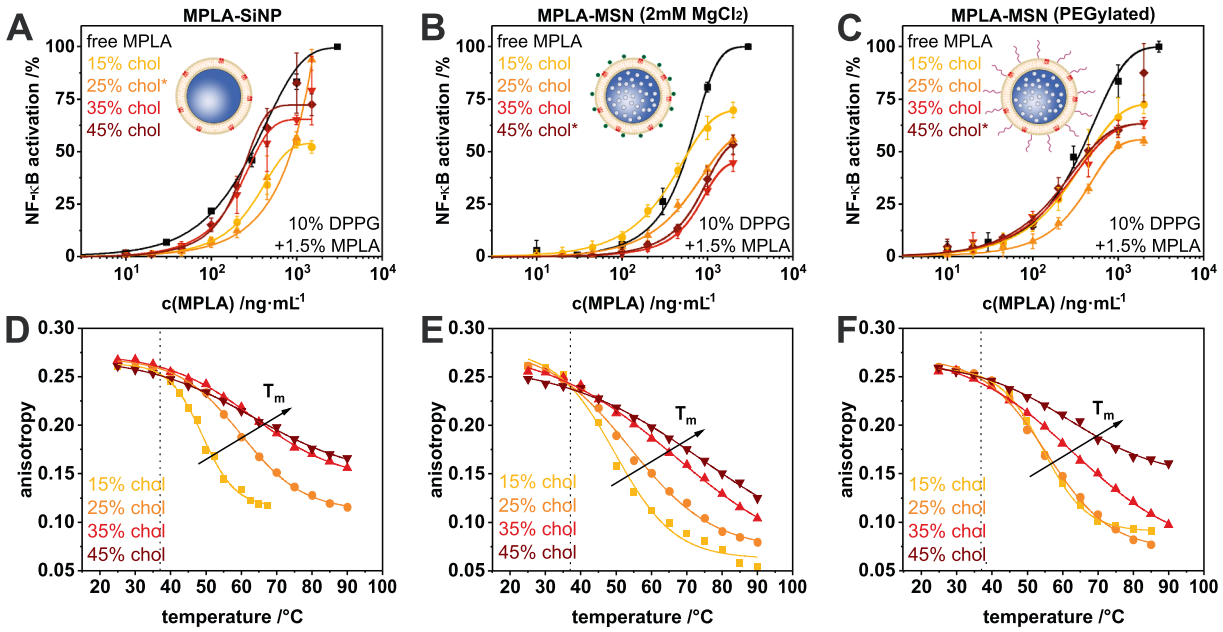

Fig. 2. Influence of cholesterol content of MPLA-SiNPs and MPLA-MSNs (stabilized either by $MgCl_2$ or PEG) on TLR4 activation and temperature-dependent membrane fluidity. The biological effect was evaluated by hTLR4 positive HEK-Blue reporter cells, and the membrane fluidity by anisotropy measurement of the fluorescent probe DPH. Particles were coated with varying cholesterol contents of 15%, 25%, 35%, or 45% (yellowish to reddish colors) in the membrane. In addition, 10% anionic DPPG and neutral DPPC were employed for lipid membrane formation. Particles were each adjuvanted with 1.5% MPLA relative to total lipid. Formulations exceeding the size limit of 200 nm are marked with an asterisk. A nonlinear regression fit model was used to generate dose–response curves. The black fitted curve represents non-formulated/free MPLA. Control particles without MPLA elicited unspecific TLR4 activation below or only low above the LOD (Fig. S5g-i). Data of the anisotropy measurement was estimated by a Boltzmann fit. A) MPLA-SiNPs required with increasing cholesterol content up to 35% decreasingly lower concentrations to elicit similar responses compared to unformulated MPLA. A further escalating cholesterol content did not lead to a significant improvement. B) MPLA-MSN_{MgCl2} showed a contrary trend. With an increasing cholesterol fraction, continuously higher particle concentrations had to be applied. All fits showed significant differences. C) The potency of MPLA-MSN_{PEG} improved with increasing cholesterol contents, however it remained consistently lower than unformulated MPLA. The nanoparticulate formulations could not be unambiguously fitted as in no case the plateau was reached. D-F) Up to physiological temperature of 37°C, membrane fluidity was comparable for all MPLA-SiNP and MPLA-MSN formulations (vertical dotted line). The trend of increasing T_m is marked by arrows. D) For MPLA-SiNPs, increasing cholesterol fraction up to 35% was accompanied by reduced fluidity. A further increase to 45% cholesterol showed no further change. E) The membrane fluidity of MPLA-MSN_{MgCl2} decreased for all formulations with increasing cholesterol fraction above a temperature of 40°C. F) Membrane fluidity of MPLA-MSN_{PEG} was similar for 15 and 25% cholesterol within the membrane and then decreased with further increasing cholesterol fraction. Data are expressed as mean ± uncertainty.

1.5% or 5% MPLA yielded the lowest EC_{50} values (100 ng/mL and 120 ng/mL, respectively).

For mesoporous MPLA-MSN_{MgCl2} increasing the DPPG content from 10% to 30% gradually increased receptor activation (Fig. 3d-f). However, in this series, particles with the highest DPPG fraction of 30% were the only formulations to fulfill the size requirement of diameters below 200 nm. These MPLA-MSN_{MgCl2} with 30% DPPG even surpassed free MPLA in TLR4 activation (Fig. 3f). As already mentioned, variation of the degree of adjuvantation did in general not lead to a strong difference between the individual dose–response curves. The lowest EC_{50} values (310–330 ng/mL) were achieved for formulations of 55:15:30 DPPC: Chol:DPPG with 1.5 and 5% MPLA adjuvantation.

For MPLA-MSN_{PEG} (Fig. 3g-i), no DPPG content showed improved receptor activation compared to unformulated MPLA. Hence a higher MPLA concentration was needed to achieve the same level of receptor activation. At 30% DPPG, MPLA-MSN_{PEG} adjuvanted with 5% MPLA performed the best among this series, however not as good as the free adjuvant.

3.4. Bayesian optimization of MPLA-SiNPs and MPLA-MSNs

Finally, data of formulations, that were developed by the classical approach by varying gradually the content of cholesterol and anionic compounds, were used to feed a BO algorithm to further improve EC_{50} values. For this purpose, the program BOXVIA (Ishii et al., 2022) was applied with two consecutive runs. Data of formulations that were proposed in the first run were fed in a second run for further optimization. The optimal formulation for each particle species that has been identified by the classical approach was directly compared to the best one suggested by BOXVIA (Fig. 4).

For solid MPLA-SiNPs, the formulation that was suggested by BO further increased TLR4 activation compared to unformulated MPLA (Fig. 4a). The EC_{50} value of the best formulation of the classical One-Factor-At-a-Time optimization approach was 150 ng/mL (45:45:10 DPPC:Chol:DPPG) compared to BO with an EC_{50} as low as 87 ng/mL (55:20:25 DPPC:Chol:DPPG). Both formulations were adjuvanted with 1.5% MPLA.

In the series of MPLA-MSNs (stabilized either with $MgCl_2$ or PEG), BO -similar to the classical approach- did not produce a significantly improved receptor activation compared to unformulated MPLA (Fig. 4b). The MPLA-MSN_{Baye} formulation suggested by the algorithm was 68.5:15:15:1.5 DPPC:Chol:DPPG:DSPE-PEG plus 1.5% MPLA without supplementation of $MgCl_2$ to the buffer. The EC_{50} value of 500 ng/mL was only slightly lower than the EC_{50} value obtained for the starting MPLA-MSN_{PEG} formulation with an EC_{50} value of 550 ng/mL, and for both MPLA-MSN formulations (classical and BO) similar concentrations of MPLA were required to elicit a similar effect compared to free/unformulated MPLA. Thus, the original MPLA-MSN_{MgCl2} formulation exhibited lowest receptor activation concentration compared to free MPLA and the other nanoparticulate formulations.

Control particles, LC-SiNPs or LC-MSNs, did not lead to unspecific TLR4 activation. The supernatant obtained after incubation with the adjuvant also elicited hardly detectable reactions proving quantitative and stable MPLA incorporation (Fig. 4c). MPLA-SiNPs and MPLA-MSN

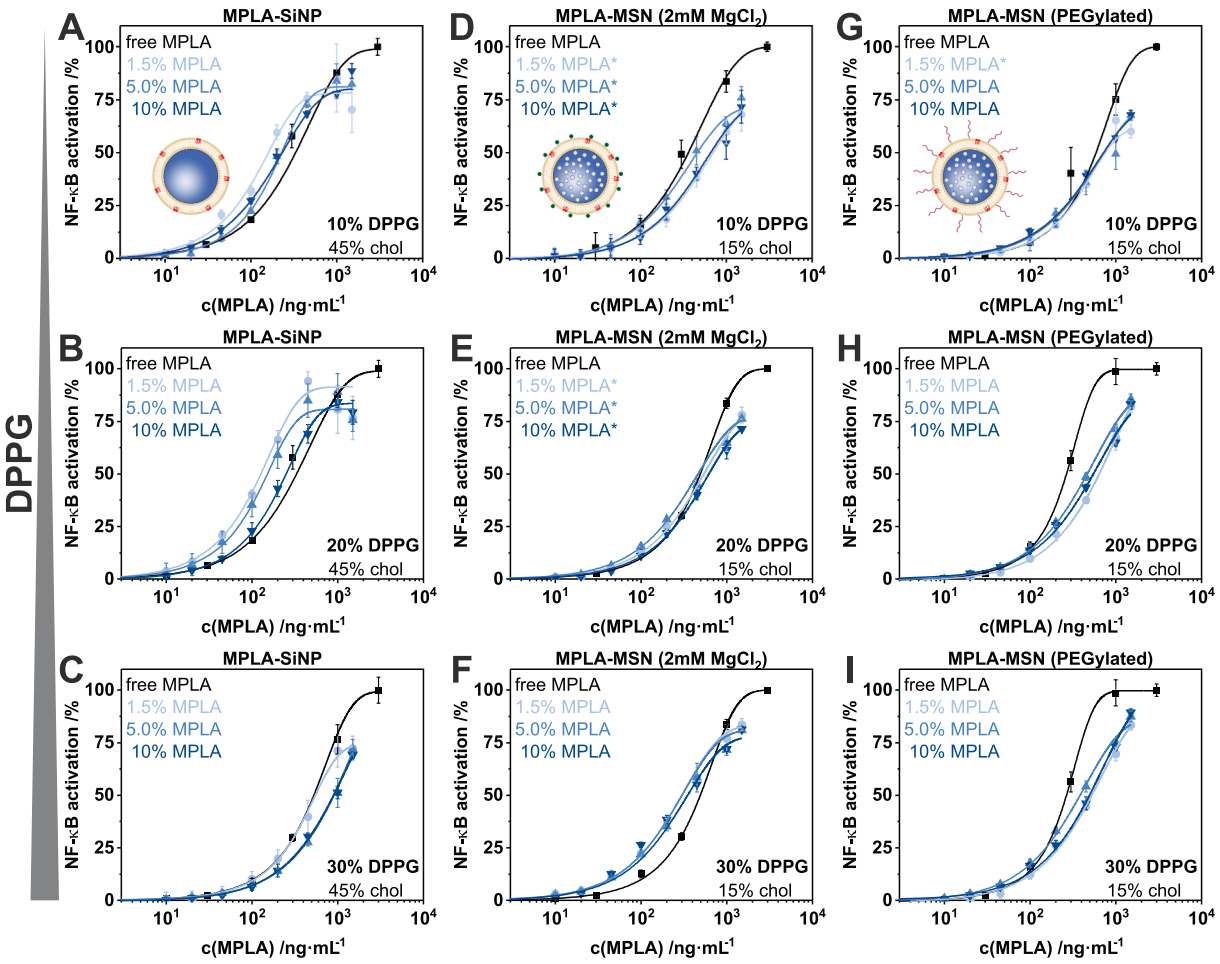

Fig. 3. Influence of the anionic compounds DPPG (10%, 20%, 30%) and MPLA (1.5%, 5%, 10%) on the biological effect of MPLA-SiNPs and MPLA-MSNs (stabilized either by $MgCl_2$ or PEG) evaluated by hTLR4 positive HEK-Blue reporter cells. Each particle series was coated with gradually increased DPPG of 10, 20 and 30% (see arrow on left side), and with cholesterol amounts as indicated in the lower right of each diagram. DPPC was added to 100%. Final particles were then adjuvanted with varying MPLA contents ranging from 1.5 to 10% (bluish colors). A nonlinear regression fit model was used to generate dose–response curves. The black fitted curves represent non-formulated adjuvant. A-C) MPLA-SiNPs elicited a higher TLR4 activation potential compared to free MPLA when fabricated with 10% or 20% DPPG, dose-response curves were shifted to the left. For MPLA-SiNPs with 30% anionic DPPG, higher MPLA concentrations were needed to elicit the same response. D-F) MPLA-MSN_{MgCl2} gradually improved cell response until particles with the highest DPPG fraction finally needed lower concentrations compared to free MPLA for the same activation. G-I) Neither variation of DPPG nor MPLA content led to improved receptor activation for MPLA-MSN_{PEG} compared to unformulated MPLA. Control particles without MPLA elicited unspecific TLR4 activation below or only slightly above the LOD (Fig. S6a). Formulations exceeding the size limit of 200 nm are marked with an asterisk. Data are expressed as mean ± uncertainty.

from both optimization methods exhibited narrow size distributions and hydrodynamic diameters of well below 200 nm thus being well suited for passive lymph node targeting. (Fig. 4d). The zeta potential of the Bayesian-optimized LC-SiNPs and classically ones were comparable with approximately −15 mV upon MPLA insertion. Adjuvantation did not affect the surface charge of LC-MSNs optimized by the Bayesian method, which remained at −12 mV pre- and post-adjuvantation. While MSN_{MgCl2}-based particles had a less pronounced charge (−9 to −9.5 mV), the zeta potential of MSN_{PEG}-based particles was at approximately −14 mV. In both classes, introduction of MPLA had no influence on the surface charge (Fig. 4e).

3.5. *In vitro uptake of LC-SiNPs by macrophages*

Macrophages play a crucial role in vaccine effectiveness by acting as antigen-presenting cells and initiating immune response. They do not only engulf and process antigens but also carry TLR4 receptors (Fu et al., 2025). Upon encountering a TLR4 ligand, macrophages recruit and activate other immune cells, release cytokines and other inflammatory mediators (Fu et al., 2025; Swanson et al., 2020). To evaluate particle engulfment and whether the liposomal membrane remains adsorbed on LC-SiNPs, the cells were incubated with LC-SiNPs carrying the optimized lipid composition as these particles exhibited the lowest EC_{50} value and imaged by confocal fluorescence microscopy (Fig. S6). Macrophages internalized increasingly more particles with increasing incubation times. Co-localization of the particle cores (green) and lipid membrane (red) was observed for early time points, as indicated by yellow spots in the merged channel for early time points. After longer incubation times, the red signal from the lipid bilayer membrane was separated from the green fluorescence of the silica particle cores, and the co-localization coefficient which decreased from 0.76 (± 0.08) to 0.45 (± 0.06) within a time range of 6 to 48 h (Fig. S7). The separation of the fluorescent signal indicates a processing of particles and lipid membranes as expected by macrophages.

4. Discussion

Adjuvants are vital for the success of protein-based vaccines especially for antigens with inherently low immunogenicity (Kaur et al., 2022; Pulendran et al., 2021; Ramezani-Rad et al., 2025). TLR agonists

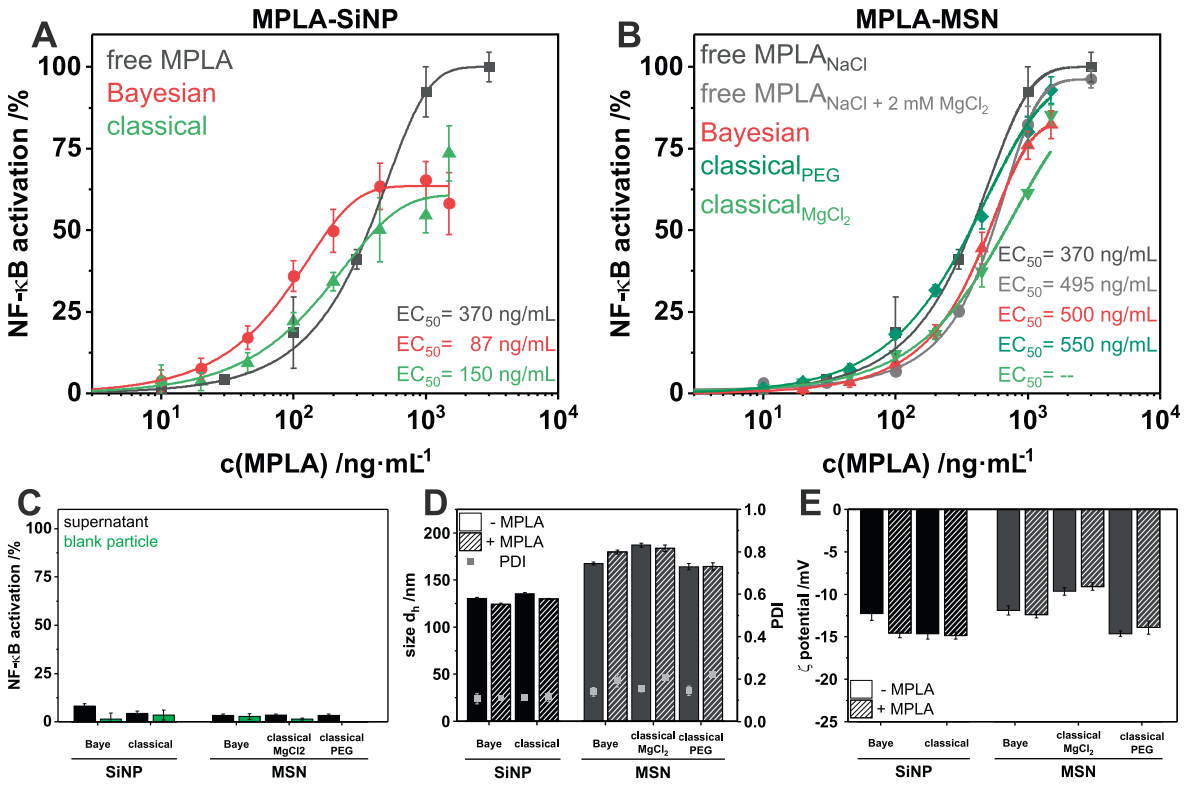

Fig. 4. Comparison of the classical one-step-at-a-time optimized and Bayesian optimized formulations of MPLA-SiNPs and MPLA-MSNs (stabilized either by $MgCl_2$ or PEG). MPLA-SiNPs and MPLA-MSNs were evaluated by hTLR4 positive HEK-Blue reporter cells. A nonlinear regression fit model was used to generate dose–response curves. The black or grey fitted curves represent non-formulated adjuvant with or without presence of $MgCl_2$. A) Bayesian-optimized particles were coated with 55:20:25 DPPC:Chol:DPPG and classically optimized particles with 45:45:10 DPPC:Chol:DPPG. Both particle species were adjuvanted with 1.5% MPLA. Both formulations reached lower EC50 values compared to free MPLA, and BO produced the formulation with the lowest overall EC50 value of 87 ng/mL. B) Bayesian-optimized MPLA-MSN_{Baye} were coated with 68.5:15:15:1.5 DPPC:Chol:DPPG:DSPE-PEG + 1.5% MPLA without supplementation of $MgCl_2$. Classically optimized particles were composed of 45:45:10 DPPC:Chol:DPPG (MPLA-MSN_{MgCl2}) and 52.5:15:30:2.5 DPPC:Chol:DPPG:DSPE-PEG + 5% MPLA (MPLA-MSN_{PEG}). All nanoparticulate formulations required higher MPLA concentrations compared to the unformulated adjuvant to achieve comparable TLR4 activation. Best one among these was classically optimized MPLA-MSN_{PEG}. Though the Bayesian formulation exhibited the lowest EC50, higher concentrations were required for the same cell response in comparison to MPLA-MSN_{PEG}. C) MPLA was quantitatively incorporated in the particles as in the particle supernatant hardly any TLR4 activation was elicited. Non-adjuvanted blank particles showed no unspecific cell activation. D) All formulations remained in the size range below 200 nm with good monodispersity as determined by DLS. Nearly no differences were noticeable for SiNP-based particles independent of the formulation. Among MSN-core particles, the size gradually increased from MPLA-MSN_{PEG} via the Bayesian-optimized formulation to MPLA-MSN_{MgCl2}. E) In contrast to the Bayesian formulation, classically optimized MPLA-SiNPs the zeta potential did not decrease compared to corresponding LC-SiNPs. For mesoporous-core particles, adjuvantation also had no effect on the zeta potential, however the formulation did. The zeta potential decreased from MPLA-MSN_{MgCl2} via the Bayesian formulation to MPLA-MSN_{PEG}. Data are expressed as mean ± uncertainty.

are frequently used as adjuvants in licensed vaccines and in research (Kaur et al., 2022; Yang et al., 2022; Alving et al., 2020; Kayesh et al., 2025; Burton et al., 2012). To harness the full potential of TLR agonists in the process of adaptive immune response, they need to be conveyed to the draining lymph nodes (Oussoren et al., 1997; Swartz et al., 2008; Reddy et al., 2007). Therefore, adjuvants should be formulated with carriers of a size preferably below 200 nm (Manolova et al., 2008). We focused on lipid-coated silica-based nanoparticles as versatile delivery platform. As supporting core, we employed either solid (SiNPs) or mesoporous (MSN) silica nanoparticles. Compared to liposomes, LC-SiNPs and LC-MSNs do not face inherent instability such as aggregation and fusion (Dhiman et al., 2022). Particles were assembled under bath sonication to assist liposome rupture followed by adsorption to the silica support. Fusion between the liposomes and the core particles occurred due to interactions between polar head groups of lipids and silanol groups (LaBauve et al., 2018; Durfee et al., 2016; Slowing et al., 2008). We chose this particle system not only because of its stability but also due to its modifiable surface, variable pore sizes and due to its tunable size (Navarro-Tovar et al., 2016; B. Vörös-Horváth, A. Salem, B. Kovács, A. Széchenyi, S. Pál, Systematic Study of Reaction Conditions for Size-Controlled Synthesis of Silica Nanoparticles, Nanomaterials (Basel, Switzerland) 14, 2024). The diameters of the coated particles were dominantly determined by the precursor silica nanoparticles. Moreover, for SiNPs and MSNs self-adjuvanticity was reported (Navarro-Tovar et al., 2016; Rithisa et al., 2024; Wan et al., 2025) which adds to the advantages of the presented platform technology. Compared to SiNPs, MSNs offer a more tunable biodegradation (Croissant et al., 2017; Zhang et al., 2024) to non-toxic silicic acid (Spitzmüller et al., 2023). The hydrolysis of silica occurs on the surface, thus the degradation rate increases with porosity, while the particle size has no significant effect for porous particles (Croissant et al., 2017).

As unsaturated lipids in bilayer membranes may reduce stability of LC-MSNs (Durfee et al., 2016), we employed saturated DPPC and DPPG for bilayer formation. Cholesterol allowed to control membrane fluidity (Subczynski et al., 2017) and DPPG ensured a negative surface charge. A negative charge was desired to avoid unspecific interaction with cells driven by electrostatic attraction at the injection site and thus depot formation (Wang et al., 2014). The determination of size, specifically the membrane thickness in cryo-TEM is a complex product of the underlying structure being convolved with the imaging process and instrument settings. The measured image intensity is not a direct reflection of the physical matter density but is modified by the Contrast Transfer

Function and the smearing effect of the 2D projection, meaning the apparent thickness can change with experimental conditions like the defocus length. Compared to DLS, the particle diameters obtained from analyses of the cryo-EM micrographs were smaller, reflecting the hydration shell. With a liposomal membrane thickness of almost 6 nm and an interfacial water layer of 3.2 nm reported in literature (Vakurov et al., 2012), the determined diameter increase of approximately 30 nm therefore fitted well to the expectation, considering also changes in the hydration shell due to the altered surface. These observations also highlight that the supported bilayer forms a highly uniform coating as the size distributions of our lipid-coated particles were governed by the silica precursor. Complete coverage was achieved by a 1.4-fold surface excess of liposomes as determined by a Langmuir adsorption isotherm. Cryo-TEM images further proved adsorption of a single lipid bilayer on LC-SiNPs and LC-MSNs. Both LC-SiNPs and LC-MSNs exhibited sizes below 200 nm, suitable for lymph node targeting, with excellent homogeneity (Fig. 1). They maintained colloidal stability at various pH values, under storage conditions at 4°C for at least one month, and at 37°C for one week, supporting their applicability for in vitro and in vivo use (Fig. S2). LC-MSNs required additional stabilization via $MgCl_2$ and/or PEGylation due to lower intrinsic stability compared to LC-SiNPs (data not shown). Surface roughness may impair lipid membrane affinity to the MSN surface thus favoring a slight tendency towards aggregation. MSNs were more negatively charged than solid SiNPs primarily because they possess a significantly larger surface area, which leads to a greater number of exposed and ionizable silanol groups (Li et al., 2021). The zeta potential of coated particles was determined by the liposomal membrane and was thus approximately similar for LC-SiNPs and LC-MSNs.

MPLA has an amphiphilic structure with a very low micelle concentration and exists therefore rather in aggregated structures in the physiological environment (Du et al., 2024). However, MPLA needs to be presented in its monomeric form to the extracellular TLR4 receptor (Du et al., 2024). We avoided aggregate formation by incorporation of MPLA into the particle's lipid bilayer membrane. In that way, we also mimicked the natural presentation of the TLR4 agonist lipopolysaccharides, of which MPLA derives are native components of gram-negative bacterial cell walls (Su et al., 2023; Ulrich and Myers, 1995). Stable incorporation of MPLA into our particle platforms was proven under storage conditions and in serum supplemented cell culture medium as none of the adjuvant leaked from the particles (Fig. S4). The high retention is not only vital for storage but also to prevent premature release of the TLR4 agonist. From the liposomal membranes adsorbed on SiNPs and MSNs, MPLA could then however still be extracted by reporter cells to stimulate TLR4.

Cholesterol influences the membrane fluidity in a bidirectional manner (Subczynski et al., 2017; Kaddah et al., 2018). Below the main phase transition temperature, it fluidizes the membrane. At high temperatures, it stabilizes the membrane and thus raises the melting point (Subczynski et al., 2017). Hence, in a first step we investigated the influence of cholesterol (15% to 45%) on its influence on MPLA extraction and thus on TLR4 activation of MPLA-SiNPs and MPLA-MSNs with the goal to reduce the EC_{50} values (Fig. 2). In solid-core MPLA-SiNPs, increasing cholesterol content from 15% to 45% led to an enhancement of TLR4 activation, as evidenced by reduced EC_{50} values and left-shifted dose–response curves. Interestingly, formulations with high cholesterol fractions of 35% and 45% achieved half-maximal activation comparable to free MPLA, although the maximal response remained lower. This suggests that cholesterol-rich membranes may facilitate better MPLA extraction, improving receptor engagement efficiency. Contrary to the trend observed in solid-core particles, mesoporous MPLA-MSN_{MgCl2} exhibited enhanced TLR4 activation at lower cholesterol levels. Formulations with 15% cholesterol showed the lowest EC_{50} values, comparable to free MPLA. Apparently, the mesoporous surface imposes additional constraints on lipid packing, thus altering lipid domain formation and MPLA orientation. Higher cholesterol content correlated with reduced receptor activation, suggesting that altered lipid organization may hinder MPLA extractability by changing the interplay with the lipids such as formation of cholesterol rich domains. Notably, the inverse relationship may also be a consequence of $MgCl_2$ as stabilization agent. Mg^{2+} ions penetrate the membrane headgroup zone and coordinate with phosphate and ester groups and cause a strong increase in the number of hydration water molecules (Alsop et al., 2016; Le et al., 2019). The resulting membrane swelling counteracts the condensing effect of cholesterol (Kaddah et al., 2018). PEGylated mesoporous MPLA-MSNs followed no cholesterol-dependent trend but exhibited overall reduced TLR4 activation. This attenuation may be attributed to steric hindrance introduced by PEGylated lipids, which could interfere with MPLA recognition. In direct comparison, the cholesterol series revealed fundamentally different behaviors: MPLA-SiNPs showed improved TLR4 activation with increasing cholesterol content, while MPLA-MSN_{MgCl2} were affected opposingly, and MPLA-MSN_{PEG} did not respond to a changing cholesterol content. These results emphasize that optimal membrane composition cannot be optimized independently of the core morphology and that also the ionic composition of the surrounding medium has to be taken into account. Membrane fluidity of particles with varying cholesterol content was assessed by DPH anisotropy. DPH inserts into the lipid bilayer where its rotational freedom is affected by the packing of the surrounding lipids. A fluid state of the membrane allows DPH to rotate more freely, decreasing its fluorescence anisotropy, while decreased fluidity restricts rotation and thus leading to higher anisotropy (Kaddah et al., 2018; Sanità et al., 2020). At physiological temperature of 37°C, variations in cholesterol content revealed no significant changes in membrane fluidity. We suspect the solid support by SiNPs or MSN to have a dominant effect to equilibrate fluidity independent of cholesterol at this temperature. Membrane fluidity did thus not contribute to MPLA extractability. The stiffening effect and resulting proportionally increase of T_m with increasing cholesterol content became only apparent at higher temperatures that are not relevant for biological systems.

In the next step, the influence of the anionic lipid DPPG and MPLA adjuvantation on TLR4 activation was examined (Fig. 3). For both MPLA-SiNPs and MPLA-MSNs variation of the MPLA loading had only a minor effect on the cell response, mildly favoring lower degrees of adjuvantation potentially due to inhibited clustering of MPLA that may occur at higher payloads. Solid-core MPLA-SiNPs with low (10%) to medium (20%) DPPG content elicited enhanced receptor activation even surpassing unformulated MPLA. A lower response for particles with 30% DPPG suggests that excessive anionic lipid may disrupt MPLA extraction possibly due to electrostatic repulsion between the particles and the cells. In contrast to solid-core particles, mesoporous MPLA-MSN_{MgCl2} formulations showed a gradual increase of TLR4 activation with rising DPPG content, suggesting that the stabilization by the divalent cation Mg^{2+} demands higher concentration of the anionic lipid. Due to the coordinated counterions, MPLA-MSN_{MgCl2} demanded higher DPPG fractions for sufficient electrostatic repulsion between each other. With too low DPPG fractions, the particles tended to aggregation (Fig. S6b), resulting in reduced cell responses. In summary, though the influence of the anionic compounds on the cell responses were not pronounced, MPLA-SiNPs performed best at low to moderate DPPG fractions, while MPLA-MSNs required high DPPG contents. Similar to the results obtained for the cholesterol variation, MPLA-MSN_{PEG} formulations exhibited no pronounced trend with alterations in the DPPG fraction. By the classical One-Factor-At-a-Time, high-cholesterol (45%) MPLA-SiNPs with a moderate fraction of the anionic lipid (20%) as well as low-cholesterol (15%) MPLA-MSNs with high DPPG contents (30%) were identified as optimal formulations. Among the tested formulations, these elicited the strongest cell responses. When directly comparing the two particle types directly, LC-SiNPs consistently outperformed LC-MSNs in terms of structural uniformity. While LC-SiNPs maintained colloidally stable under most tested conditions, LC-MSNs showed a higher tendency toward aggregation. Notably, effective TLR4 activation required not

only the presence of the adjuvant, but also the availability of MPLA in an "extractable" form from both MPLA-SiNPs and MPLA-MSNs.

To refine the immunostimulatory performance of lipid-coated silica nanoparticles, we applied as last step a BO strategy using the program BOXVIA (Ishii et al., 2022). Classical optimizations neglect interactions between the individual variables. BO can overcome this drawback and take interactions of the individual parameters into account. This approach aimed to minimize EC_{50} values for TLR4 activation by leveraging prior experimental data from classical stepwise optimization of cholesterol and content of anionic compounds. Additionally, the concentration of $MgCl_2$ added to the buffer and the degree of PEGylation of MPLA-MSNs became variables because $MgCl_2$ can interfere with TLR4/NF-κB signaling pathway (Hu et al., 2018; He et al., 2023). For solid-core MPLA-SiNPs, BO yielded a formulation with a notably lower EC_{50} (87 ng/mL) compared to the best classical formulation (150 ng/mL). This improvement indicates that the algorithm successfully identified a more effective balance of lipid components, enhancing MPLA presentation and receptor engagement. However, BO did not significantly improve the performance of mesoporous MPLA-MSNs. The suggested formulation achieved a modest reduction in EC_{50} (from 550 ng/mL to 500 ng/mL) compared to the best-performing formulation of the classical optimization approach. As the classical formulation elicited stronger cell responses at equivalent concentrations, these findings suggest that the algorithm may have prioritized EC_{50} minimization at the expense of overall activation potential. The limited improvement observed for MPLA-MSNs suggests that their design space is more complex and may involve non-linear interactions between porosity, surface charge and membrane composition. In contrast, the more predictable behavior and fewer parameters of MPLA-SiNPs, as there was no PEGylation or supplementation of divalent ions required, allowed BO to identify a formulation with substantially improved EC_{50}. In summary, solid MPLA-SiNPs were with enhanced TLR4 activation superior to their mesoporous counterparts. If this is also true for other adjuvants needs to be evaluated in future studies. Moreover, in this study functional assessments of TLR4 activation were performed in vitro using reporter cells, neglecting the complex fate of particles in a living organisms, such as protein adsorption, the interaction with a variety of immune cell and with off-target cells.

For further research we suggest a dual delivery of adjuvants with immunogens. Macrophages are central to initiating and shaping immune responses due to their dual role in antigen processing and expression of pattern recognition receptors such as TLR4 (Fu et al., 2025). Therefore, understanding how macrophages interact with and process adjuvanted nanoparticles is critical for evaluating their immunological potential. The cells did not only readily internalize LC-SiNPs but also processed them (Fig. 5). Early co-localization of the lipid bilayer membrane and silica core indicated intact particle structures during initial uptake. Following progressive separation of these signals and the corresponding decrease in co-localization coefficient suggest that the lipid membrane is gradually degraded or processed intracellularly. The particle

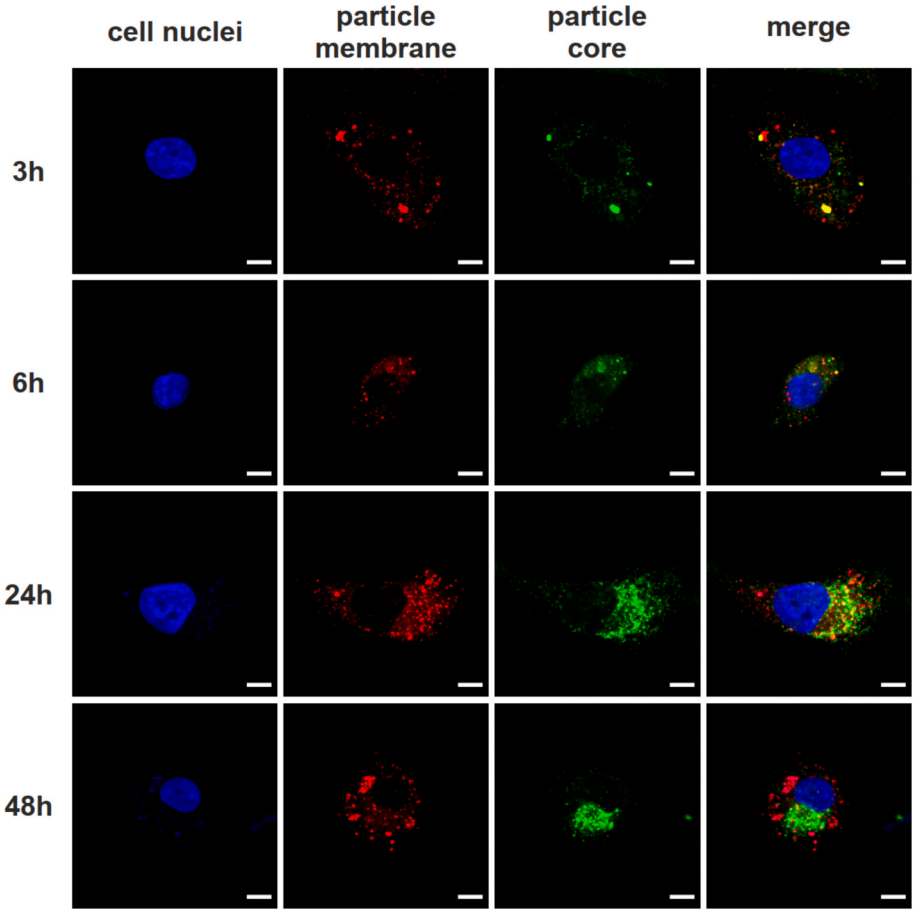

Fig. 5. Confocal microscopy images of macrophages incubated with LC-SiNPs over a time range of 3–48 h. Macrophages were differentiated from THP-1 cells via PMA stimulation for 48 h. Resulting macrophages were exposed to LC-SiNPs at a concentration equivalent to 500 ng/mL, corresponding to the plateau of maximal TLR4 activation in the reporter assay. Beyond that particle concentration, increases in dose did not enhance the cellular response. Cell nuclei were stained with DAPI (blue), liposomal particle membranes with DiD (red) and green fluorescent SiNP cores were employed. Yellow signals in the merged channel indicate colocalization of the particle membranes and cores and thus intact LC-SiNPs with adsorbed liposomal membranes. At early time points, limited particle uptake resulted in few but colocalized signals. With prolonged incubation, particle engulfment increased, accompanied by progressive spatial separation of red and green signals as evidenced by diminished yellow spots. The size bar represents 10 μm.

disassembly suggests a favorable balance between extracellular stability and intracellular degradability. The temporal dissociation of the lipid shell from the particle core is with outlook to a potential dual antigen and adjuvant delivery a promising indicator of successful intracellular processing, which is essential for antigen presentation and subsequent immune response (Muntjewerff et al., 2020). Even though we lack studies of the intracellular processing mechanisms, these findings support the suitability of the particle system for vaccine applications, particularly in delivering both adjuvants and antigens.

5. Conclusion and outlook

This study presents a systematic and multi-layered approach to optimizing lipid-coated silica nanoparticles (LC-SiNPs and LC-MSNs) as versatile carriers for TLR agonists with the goal of enhancing immunostimulatory performance for vaccine applications. The modular platform can in future also be exploited for various TLR agonists. For example, other amphiphilic TLR agonists like Pam_3CSK_4 (TLR1/2 agonist) (Zhou et al., 2024) may be inserted into the membrane similar to MPLA, or hydrophilic ones such as imidazoquinoline (TLR7/8 agonist) could alternatively be covalently coupled to phospholipid head groups on the particle surface (Miller et al., 2020). In addition, the delivery platform would also allow for covalent attachment of antigens by incorporating lipids with functional head groups into liposomal membranes.

CRediT authorship contribution statement

Andreas G. Schreiber: Writing – review & editing, Writing – original draft, Visualization, Methodology, Investigation, Formal analysis, Data curation, Conceptualization. **Johannes Konrad:** Methodology. **Renate Liebl:** Methodology. **Bastian Beitzinger:** Methodology. **Jan Krutina:** Methodology. **Gregor Madej:** Methodology. **Mika Lindén:** Writing – review & editing, Supervision. **Christine Ziegler:** Writing – review & editing, Supervision. **Miriam Breunig:** Writing – review & editing, Supervision, Investigation, Funding acquisition, Conceptualization.

Declaration of competing interest

The authors declare that they have no known competing financial interests or personal relationships that could have appeared to influence the work reported in this paper.

Acknowledgments

This work was supported by the Deutsche Forschungsgemeinschaft (DFG), grant No BR 3566/5–1. The authors want to gracefully thank Lipoid GmbH for donations of phospholipids. We thank Yana Gorbatii and Merve Gökalp for excellent technical assistance.

Appendix A. Supplementary data

Supplementary data to this article can be found online at https://doi.org/10.1016/j.ijpharm.2026.126629.

Data availability

Data will be made available on request.

References

Akar, S., Fardindoost, S., Hoorfar, M., 2024. High throughput microfluidics-based synthesis of PEGylated liposomes for precise size control and efficient drug encapsulation, Colloids and surfaces. B, Biointerfaces 238, 113926.
Alsop, R.J., Maria Schober, R., Rheinstädter, M.C., 2016. Swelling of phospholipid membranes by divalent metal ions depends on the location of the ions in the bilayers. Soft Matter 12, 6737–6748.
Alving, C.R., Peachman, K.K., Matyas, G.R., Rao, M., Beck, Z., 2020. Army Liposome Formulation (ALF) family of vaccine adjuvants. Expert Rev. Vaccines 19, 279–292.
Barbey, C., Su, J., Billmeier, M., Stefan, N., Bester, R., Carnell, G., Temperton, N., Heeney, J., Protzer, U., Breunig, M., Wagner, R., Peterhoff, D., 2023. Immunogenicity of a silica nanoparticle-based SARS-CoV-2 vaccine in mice. Eur. J. Pharm. Biopharm. 192, 41–55.
Botos, I., Segal, D.M., Davies, D.R., 2011. The structural biology of Toll-like receptors. Structure 19, 447–459.
Burton, D.R., Ahmed, R., Barouch, D.H., Butera, S.T., Crotty, S., Godzik, A., Kaufmann, D. E., McElrath, M.J., Nussenzweig, M.C., Pulendran, B., Scanlan, C.N., Schief, W.R., Silvestri, G., Streeck, H., Walker, B.D., Walker, L.M., Ward, A.B., Wilson, I.A., Wyatt, R., 2012. A Blueprint for HIV Vaccine Discovery. Cell Host Microbe 12, 396–407.
Croissant, J.G., Fatieiev, Y., Khashab, N.M., 2017. Degradability and Clearance of Silicon, Organosilica, Silsesquioxane, Silica mixed Oxide, and Mesoporous Silica Nanoparticles, Advanced materials (Deerfield Beach. Fla.) 29.
D'Onofrio, V., Santana, A.C., Pauwels, M., Waerlop, G., Willems, A., de Boever, F., Müller, M., Sehr, P., Waterboer, T., Leroux-Roels, I., Sharma, A.A., Sékaly, R.P., Leroux-Roels, G., 2025. AS04 drives superior cross-protective antibody response by increased NOTCH signaling of dendritic cells and proliferation of memory B cells. Front. Immunol. 16, 1623405.
Dhiman, N., Sarvaiya, J., Mohindroo, P., 2022. A drift on liposomes to proliposomes: recent advances and promising approaches. J. Liposome Res. 32, 317–331.
Du, Y., Lv, J., Hao, Z., Li, Z., Song, T., Ge, H., Wang, H., Yu, Z., Xie, Z., Li, D., Liu, Y., 2024. Pickering emulsion-guided monomeric delivery of monophosphoryl lipid a for enhanced vaccination. J. Control. Release 374, 39–49.
Durfee, P.N., Lin, Y.-S., Dunphy, D.R., Muñiz, A.J., Butler, K.S., Humphrey, K.R., Lokke, A.J., Agola, J.O., Chou, S.S., Chen, I.-M., Wharton, W., Townson, J.L., Willman, C.L., Brinker, C.J., 2016. Mesoporous Silica Nanoparticle-Supported Lipid Bilayers (Protocells) for active Targeting and delivery to Individual Leukemia Cells. ACS Nano 10, 8325–8345.
Friedman-Klabanoff, D.J., Jensen, T.L., Gelber, C.E., Pinapati, R.S., Tan, J.C., Deye, G.A., Regules, J.A., Bergmann-Leitner, E.S., Laurens, M.B., Travassos, M.A., Goll, J.B., Takala-Harrison, S., Berry, A.A., 2025. Vaccine-induced antibodies to a C-terminal *Plasmodium falciparum* circumsporozoite protein epitope are associated with protection. J Infect Dis.
Fu, Y., Gong, T., Loughran, P.A., Li, Y., Billiar, T.R., Liu, Y., Wen, Z., Fan, J., 2025. Roles of TLR4 in macrophage immunity and macrophage-pulmonary vascular/lymphatic endothelial cell interactions in sepsis. Commun. Biol. 8, 469.
Gisperg, F., Klausser, R., Elshazly, M., Kopp, J., Brichtová, E.P., Spadiut, O., 2025. Bayesian Optimization in Bioprocess Engineering-where do we stand today? Biotechnol. Bioeng. 122, 1313–1325.
Gu, Z., Yin, J., Da Silva, C.G., Liu, Q., Cruz, L.J., Ossendorp, F., Snaar-Jagalska, E., 2024. Therapeutic liposomal combination to enhance chemotherapy response and immune activation of tumor microenvironment. J. Control. Release 373, 38–54.
Hamid, F.A., Le, N.-M.-N., Song, D., Amin, H., Hicks, L., Bird, S., Siram, K., Hoppe, B., Demeler, B., Evans, J.T., Burkhart, D.J., Pravetoni, M., 2025. A novel cationic liposome-formulated toll like receptor (TLR) 7/8 agonist enhances the efficacy of a vaccine against fentanyl toxicity. J. Control. Release 384, 113901.
He, W., 2023. DPH Probe Method for Liposome-Membrane Fluidity Determination, Methods in molecular biology (Clifton. N.J.) 2622, 241–244.
He, X., Bai, Q., Zhang, X., Zhang, L., 2023. MgCl2 Attenuates ox-LDL-Induced Vascular Smooth Muscle-Derived Foam Cells Pyroptosis by Downregulating the TLR4/NF-κB Signaling Pathway. Biol. Trace Elem. Res. 201, 5242–5256.
Hernán-García, C., Sánchez-Carmona, D.L., Mateo-Otero, L.C., Fernández-Espinilla, V., Rodriguez-Ducuara, P.A., Castrodeza-Sanz, J.J., Prada-García, C., 2025. Immunogenicity and predictive factors of hepatitis B vaccination with Fendrix® in chronic kidney disease patients. Front. Public Health 13, 1523733.
Hood, R.R., DeVoe, D.L., 2015. High-Throughput Continuous Flow production of Nanoscale Liposomes by Microfluidic Vertical Flow focusing. Small 11, 5790–5799.
Hu, T., Xu, H., Wang, C., Qin, H., An, Z., 2018. Magnesium enhances the chondrogenic differentiation of mesenchymal stem cells by inhibiting activated macrophage-induced inflammation. Sci. Rep. 8, 3406.
Ignacio, B.J., Albin, T.J., Esser-Kahn, A.P., Verdoes, M., 2018. Toll-like Receptor Agonist Conjugation: a Chemical Perspective. Bioconjug. Chem. 29, 587–603.
Ishii, A., Kamijyo, R., Yamanaka, A., Yamamoto, A., 2022. BOXVIA: Bayesian optimization executable and visualizable application. SoftwareX 18, 101019.
Kaddah, S., Khreich, N., Kaddah, F., Charcosset, C., Greige-Gerges, H., 2018. Cholesterol modulates the liposome membrane fluidity and permeability for a hydrophilic molecule. Food Chem. Toxicol. 113, 40–48.
Kaur, A., Baldwin, J., Brar, D., Salunke, D.B., Petrovsky, N., 2022. Toll-like receptor (TLR) agonists as a driving force behind next-generation vaccine adjuvants and cancer therapeutics. Curr. Opin. Chem. Biol. 70, 102172.
Kayesh, M.E.H., Kohara, M., Tsukiyama-Kohara, K., 2025. Toll-like Receptor (TLR) Response in Chikungunya Virus Infection: Mechanism of Activation. Immune Evasion, and Use of TLR Agonists in Vaccine Development, Vaccines 13, 856.
LaBauve, A.E., Rinker, T.E., Noureddine, A., Serda, R.E., Howe, J.Y., Sherman, M.B., Rasley, A., Brinker, C.J., Sasaki, D.Y., Negrete, O.A., 2018. Lipid-Coated Mesoporous Silica Nanoparticles for the delivery of the ML336 Antiviral to Inhibit Encephalitic Alphavirus Infection. Sci. Rep. 8, 13990.
Laupèze, B., Hervé, C., Di Pasquale, A., Da Tavares Silva, F., 2019. Adjuvant Systems for vaccines: 13 years of post-licensure experience in diverse populations have

progressed the way adjuvanted vaccine safety is investigated and understood. Vaccine 37, 5670–5680.
Le, C.T.M., Houri, A., Balage, N., Smith, B.J., Mechler, A., 2019. Interaction of Small Ionic Species with Phospholipid Membranes: the Role of Metal Coordination. Front. Mater. 5, 401354.
Li, J., Shen, S., Kong, F., Jiang, T., Tang, C., Yin, C., 2018. Effects of pore size on in vitro and in vivo anticancer efficacies of mesoporous silica nanoparticles. RSC Adv. 8, 24633–24640.
Li, Y., Du, N., Song, S., Hou, W., 2021. Size-dependent dissociation of surface hydroxyl groups of silica in aqueous solution. Colloids Surf A Physicochem Eng Asp 629, 127446.
Liu, Z., Zhou, C., Qin, Y., Wang, Z., Wang, L., Wei, X., Zhou, Y., Li, Q., Zhou, H., Wang, W., Fu, Y.-X., Zhu, M., Liang, W., 2017. Coordinating antigen cytosolic delivery and danger signaling to program potent cross-priming by micelle-based nanovaccine. Cell Discov 3, 17007.
Manolova, V., Flace, A., Bauer, M., Schwarz, K., Saudan, P., Bachmann, M.F., 2008. Nanoparticles target distinct dendritic cell populations according to their size. Eur. J. Immunol. 38, 1404–1413.
Miller, S.M., van Cybulski, M., Whitacre, L.S., Bess, M.T., Livesay, L., Walsh, D., Burkhart, H.G., Bazin, J.T.E., 2020. Novel Lipidated Imidazoquinoline TLR7/8 Adjuvants Elicit Influenza-specific Th1 Immune responses and Protect against Heterologous H3N2 Influenza Challenge in mice. Front. Immunol. 11, 406.
Mizuta, R., Inoue, F., Sasaki, Y., Sawada, S.-I., Akiyoshi, K., 2023. A Facile Method to Coat Nanoparticles with Lipid Bilayer Membrane: Hybrid Silica Nanoparticles Disguised as Biomembrane Vesicles by Particle Penetration of Concentrated Lipid Layers. Small 19, e2206153.
Moura, S.P., Carmona-Ribeiro, A.M., 2005. Biomimetic particles: optimization of phospholipid bilayer coverage on silica and colloid stabilization. Langmuir the ACS Journal of Surfaces and Colloids 21, 10160–10164.
Muntjewerff, E.M., Meesters, L.D., van den Bogaart, G., 2020. Antigen Cross-Presentation by Macrophages. Front. Immunol. 11, 1276.
Navarro-Tovar, G., Palestino, G., Rosales-Mendoza, S., 2016. An overview on the role of silica-based materials in vaccine development. Expert Rev. Vaccines.
Naz, F., Hagspiel, N., Xu, F., Thompson, B., Brett Moreau, G., Young, M., Herbein, J., Fox, C.B., Petri, W.A., Abhyankar, M.M., 2025. Enhanced immunogenicity of a Clostridioides difficile TcdB vaccine adjuvanted with a synthetic dual-TLR ligand adjuvant. npj Vaccines 10, 33.
Nsairat, H., Khater, D., Sayed, U., Odeh, F., Al Bawab, A., Alshaer, W., 2022. Liposomes: structure, composition, types, and clinical applications. Heliyon 8, e09394.
Oussoren, C., Zuidema, J., Crommelin, D., Storm, G., 1997. Lymphatic uptake and biodistribution of liposomes after subcutaneous injection. Biochim. Biophys. Acta Biomembr. 1328, 261–272.
Patel, P., Santo, K.P., Burgess, S., Vishnyakov, A., Neimark, A.V., 2020. Stability of Lipid Coatings on Nanoparticle-decorated Surfaces. ACS Nano 14, 17273–17284.
Peletta, A., Lemoine, C., Courant, T., Collin, N., Borchard, G., 2023. Meeting vaccine formulation challenges in an emergency setting: Towards the development of accessible vaccines. Pharmacol. Res. 189, 106699.
Pulendran, B., Arunachalam, P.S., O'Hagan, D.T., 2021. Emerging concepts in the science of vaccine adjuvants. Nat. Rev. Drug Discov. 20, 454–475.
Ramezani-Rad, P., Marina-Zárate, E., Maiorino, L., Myers, A., Kaczmarek Michaels, K., Pires, I.S., Bloom, N.I., Melo, M.B., Lemnios, A.A., Lopez, P.G., Cottrell, C.A., Burton, I., Groschel, B., Pradhan, A., Stiegler, G., Budai, M., Kumar, D., Pallerla, S., Sayeed, E., Sagar, S.L., Kasturi, S.P., van Rompay, K.K., Hangartner, L., Wagner, A., Burton, D.R., Schief, W.R., Crotty, S., Irvine, D.J., 2025. The saponin monophosphoryl lipid a nanoparticle adjuvant induces dose-dependent HIV vaccine responses in nonhuman primates. The Journal of Clinical Investigation 135.
Reddy, S.T., van der Vlies, A.J., Simeoni, E., Angeli, V., Randolph, G.J., O'Neil, C.P., Lee, L.K., Swartz, M.A., Hubbell, J.A., 2007. Exploiting lymphatic transport and complement activation in nanoparticle vaccines. Nat. Biotechnol. 25, 1159–1164.
Rithisa, B., Gowsalya, K., Abdul Rasheed, P., Vivek, R., 2024. Recent progress in smart inorganic mesoporous silica-based nanovaccine for cancer. Inorg. Chem. Commun. 164, 112483.
Sanità, G., Carrese, B., Lamberti, A., 2020. Nanoparticle Surface Functionalization: how to Improve Biocompatibility and Cellular Internalization. Front. Mol. Biosci. 7, 587012.
Slowing, I.I., Vivero-Escoto, J.L., Wu, C.-W., Lin, V.-S.-Y., 2008. Mesoporous silica nanoparticles as controlled release drug delivery and gene transfection carriers. Adv. Drug Deliv. Rev. 60, 1278–1288.
Spitzmüller, L., Nitschke, F., Rudolph, B., Berson, J., Schimmel, T., Kohl, T., 2023. Dissolution control and stability improvement of silica nanoparticles in aqueous media. J. Nanopart. Res. 25.
Subczynski, W.K., Pasenkiewicz-Gierula, M., Widomska, J., Mainali, L., Raguz, M., 2017. High Cholesterol/Low Cholesterol: Effects in Biological Membranes: a Review. Cell Biochem. Biophys. 75, 369–385.
Su, S., Chen, L., Yang, M., Liang, D., Ke, B., Liu, Z., Ke, C., Liao, G., Liu, L., Luo, X., 2023. Design, synthesis and immunological evaluation of monophosphoryl lipid a derivatives as adjuvants for a RBD-hFc based SARS-CoV-2 vaccine. RSC Med. Chem. 14, 47–55.
Swanson, L., Katkar, G.D., Tam, J., Pranadinata, R.F., Chareddy, Y., Coates, J., Anandachar, M.S., Castillo, V., Olson, J., Nizet, V., Kufareva, I., Das, S., Ghosh, P., 2020. TLR4 signaling and macrophage inflammatory responses are dampened by GIV/Girdin. PNAS 117, 26895–26906.
Swartz, M.A., Hubbell, J.A., Reddy, S.T., 2008. Lymphatic drainage function and its immunological implications: from dendritic cell homing to vaccine design. Semin. Immunol. 20, 147–156.
Thalhauser, S., Peterhoff, D., Wagner, R., Breunig, M., 2020. Presentation of HIV-1 Envelope Trimers on the Surface of Silica Nanoparticles. J. Pharm. Sci. 109, 911–921.
Ulrich, J.T., Myers, K.R., 1995. Monophosphoryl lipid a as an adjuvant. Past Experiences and New Directions, Pharmaceutical Biotechnology 6, 495–524.
Vakurov, A., Brydson, R., Nelson, A., 2012. Electrochemical modeling of the silica nanoparticle-biomembrane interaction. Langmuir the ACS Journal of Surfaces and Colloids 28, 1246–1255.
Vörös-Horváth, B., Salem, A., Kovács, B., Széchenyi, A., Pál, S., 2024. Systematic Study of Reaction Conditions for Size-Controlled Synthesis of Silica Nanoparticles. Nanomaterials (Basel, Switzerland) 14.
Wan, H., Yang, Y., Tu, Z., Tang, M., Jing, B., Feng, Y., Xie, J., Gao, H., Song, X., Zhao, X., 2025. Enhanced mucosal immune response through nanoparticle delivery system based on chitosan-catechol and a recombinant antigen targeted towards M cells. Int. J. Biol. Macromol. 141345.
Wang, C., Liu, P., Zhuang, Y., Li, P., Jiang, B., Pan, H., Liu, L., Cai, L., Ma, Y., 2014. Lymphatic-targeted cationic liposomes: a robust vaccine adjuvant for promoting long-term immunological memory. Vaccine 32, 5475–5483.
Yang, J.-X., Tseng, J.-C., Yu, G.-Y., Luo, Y., Huang, C.-Y.-F., Hong, Y.-R., Chuang, T.-H., 2022. Recent advances in the Development of Toll-like Receptor Agonist-based Vaccine Adjuvants for Infectious Diseases. Pharmaceutics 14.
Zhang, Y., Lin, X., Chen, X., Fang, W., Yu, K., Gu, W., Wei, Y., Zheng, H., Piao, J., Li, F., 2024. Strategies to Regulate the Degradation and Clearance of Mesoporous Silica Nanoparticles: a Review. Int. J. Nanomed. 19, 5859–5878.
Zhou, S.-H., Zhang, R.-Y., Wen, Y., Zou, Y.-K., Ding, D., Bian, M.-M., Cui, H.-Y., Guo, J., 2024. Multifunctional Lipidated Protein Carrier with a Built-In Adjuvant as a Universal Vaccine Platform Potently Elevates Immunogenicity of Weak Antigens. J. Med. Chem. 67, 6822–6838.
Zimmermann, J., Goretzki, A., Meier, C., Wolfheimer, S., Lin, Y.-J., Rainer, H., Krause, M., Wedel, S., Spies, G., Führer, F., Vieths, S., Scheurer, S., Schülke, S., 2022. Modulation of dendritic cell metabolism by an MPLA-adjuvanted allergen product for specific immunotherapy. Front. Immunol. 13, 916491.